JOURNAL OF CATALYSIS 134, 422–433 (1992)

On the Active Site of MgO/CaO Mixed Oxide for Oxidative Coupling of Methane

R. PHILIPP,[1] K. OMATA, A. AOKI, AND K. FUJIMOTO[2]

Department of Synthetic Chemistry, Faculty of Engineering, The University of Tokyo, Hongo, Bunkyo-ku, Tokyo 113, Japan

Received February 20, 1991; revised September 3, 1991

The catalytic performance of Mg/Ca mixed oxides for oxidative coupling of methane and their physical properties were studied. It was found that while the activity for formation of carbon oxides was not influenced by the ratio MgO/CaO, both selectivity and activity to C_2 hydrocarbons were maximum (67% and 14.5 C-mmol · h^{-1} · g^{-1}, respectively) with 85% MgO/CaO at 1023 K. The values increased with increasing reaction temperature. Physical properties such as the strain in the MgO lattice and the amount of strongly adsorbed CO_2 were also maximum at the same composition. It was found that most of the surface species was MgO for Mg-rich oxides. Surface basicity, which was estimated by the wavenumber difference of the asymmetric and symmetric IR absorption bands of surface carbonates, was associated with these properties. The basicity of MgO, which was promoted by incorporated CaO, is considered to be the main factor for promoting the coupling activity.

INTRODUCTION

Alkaline earth metal oxides, especially MgO, have long been known to be active catalysts for oxidative coupling of methane. It has been pointed out that both the selectivity for C_2 hydrocarbons and the basicity of alkaline earth metal oxides are in the order: BeO < MgO < CaO < SrO < BaO (*1*, *2*). It has also been reported that MgO shows higher selectivity for C_2 hydrocarbons when alkali compounds are doped (*3*). Li-doped MgO represents a special category among these catalysts (e.g., (*4–6*)). Matsuda *et al.* (*7*) reported that basicity measured by phenol adsorption increased by incorporation of $NaBH_4$ or $NaNH_2$ on MgO. These facts suggest that the basicity of catalyst is essential for high selectivity to C_2 hydrocarbons.

Other additives in alkaline earth metal oxides such as Li_2CO_3 (*4*), $RbNO_3$ (*3*), $Ba(OH)_2$, (*8*), $La(NO_3)_3$, (*9*), and $CaCl_2$ (*10*) are also known to be effective in promoting catalytic performance. A variety of functions of additives has been proposed for high selectivity, such as to form active centers (*4*), to form structural defects resulting in oxygen species of low coordination (*9*), to form lattice distortion, and to reduce surface area (*3*).

Mixed oxides of CaO/MgO or Ca^{2+}-doped MgO have been reported to show high activity and selectivity for oxidative methane coupling (*11*, *12*). It was reported that Ca^{2+}-doped MgO shows higher basicity than pure MgO (*13*) and a previous paper (*12*) we clarified the significant relationship between the activity and basicity of the mixed oxide catalyst. The present study has been undertaken to clarify the morphology of mixed MgO/CaO oxides and to correlate their catalytic performances with their physical properties.

EXPERIMENTAL

Catalyst Preparation

MgO, CaO, and several mixed oxides with different composition (mostly 95 mol%

[1] On leave from the Central Institute of Physical Chemistry, Berlin, Germany.

[2] To whom all correspondence should be addressed.

0021-9517/92 $3.00

MgO/CaO, 85 mol% MgO/CaO, 75 mol% MgO/CaO, 50 mol% MgO/CaO, and 25 mol% MgO/CaO) were used. Catalysts were prepared by coprecipitating hydroxides from aqueous solution of the corresponding nitrates ($Ca(NO_3)_2 4H_2O$; $Mg(NO_3)_2 6H_2O$; Koso Chemical Co. Ltd., guaranteed grade, used without further purification) by the addition of sodium hydroxide at 323 K, subsequent washing with water, and drying in air at 393 K. They were activated by calcining in air at 1023 K for 30 min before reaction or CO_2 TPD measurement.

Reaction Apparatus and Procedures

Methane oxidation was conducted in a fixed-bed, flow-type reaction apparatus. A quartz tube (6-mm i.d.) was employed as a reactor where 0.3 g of catalyst was charged for activity measurements and 0.015 g of catalyst for measurements of kinetics. The details of the reaction apparatus have been described in a previous paper (*10*). The reaction conditions were: temperature = 1003–1103 K, W/F = 0.02-1 g-cat · h · mol^{-1}, P_{CH_4} = 13–35 kPa, P_{O_2} = 1.4–5.7 kPa. Effluent gas was analyzed by on-line gas chromatography. CO and CO_2 in the product gas were converted to methane in a methanator (Ru/Al_2O_3 catalyst, 723 K) and then detected by FID.

Catalyst Characterization

a. CO_2 adsorption and TPD. Volumetric measurement of CO_2 adsorption and temperature-programed desorption (TPD) of CO_2 were carried out to investigate surface basicity. A sample was heated at 1023 K in flowing air for 30 min followed by evacuation at that temperature. After cooling to room temperature, 20 kPa of CO_2 was introduced onto the sample. Evacuation and CO_2 introduction (13.3 kPa) were repeated to distinguish physical and chemical adsorption volumetrically. After conducting the measurement the sample was subjected to TPD *in situ* at a heating rate of 10 K · min^{-1} up to 1073 K in flowing He. The effluent gas was analyzed by on-line gas chromatography.

b. Surface area. Specific surface area was determined by the BET method with a Quantasorb instrument (Yuasa Ionics) using helium gas containing 30% nitrogen.

c. IR spectroscopic measurement. The FTIR measurements were performed with a Perkin–Elmer 1600 Series FTIR instrument at room temperature. The transmission absorption technique was applied in the range 4000–900 cm^{-1}. The oxides were pressed into thin self-supporting sample wafers. The IR cell was homemade. It had cemented CaF_2 windows and permitted all sample handling to be performed without removing the oxide wafers from the cell. The wafers were calcined in the heating zone of the cell at 1223 K for 45 min in flowing helium. The calcined samples were moved into the optical path and cooled to room temperature in a helium atmosphere. They were exposed to a CO_2 stream for 10 min. Surplus of CO_2 was removed by purging with helium. A set of desorption experiments was carried out by heating the disks on which CO_2 was previously adsorbed at a fixed temperature for 10 min in a helium stream. After cooling to room temperature the corresponding spectrum was recorded and the procedure was repeated with continuously increasing desorption temperatures.

d. XRD measurement. XRD measurements were conducted with a Rigaku Rotaflex instrument using Cu$K\alpha$ irradiation (40 kV, 100 mV). The catalyst powder was calcined at 1073 K for 1 h immediately before measurement.

RESULTS AND DISCUSSION

Catalytic Features of CaO/MgO Catalyst

a. Effects of catalyst composition. Conversion rates of methane to C_2 (C_2H_6 and C_2H_4) and CO_x (CO and CO_2) at 1023 K are illustrated in Fig. 1. The MgO composition ranges from 0 to 100 mol%. While methane conversion to C_2 and CO_x was 9.2 and 4.4%, respectively, with 85% MgO/CaO catalyst, the conversions were 0.5 and 0.5%, respec-

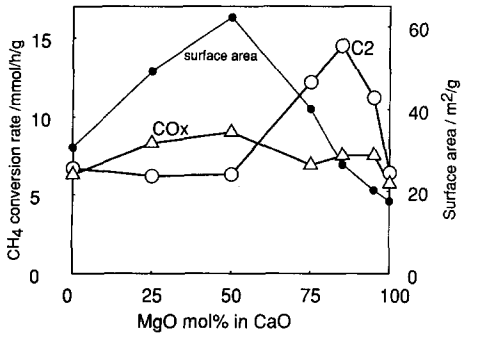

FIG. 1. Catalytic activity and specific surface areas of MgO/CaO catalysts: T = 1023 K, W/F = 1 g-cat · h · mol^{-1}, P_{CH_4} = 13.1, P_{O_2} = 1.4, P_{N_2} = 86.5 kPa.

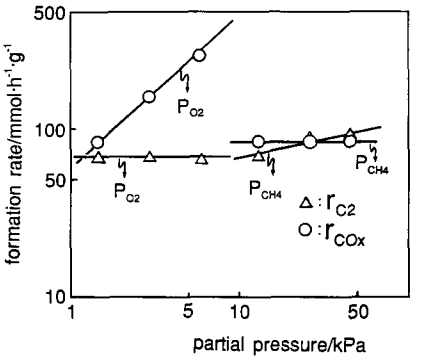

FIG. 2. Kinetics with 85 mol% MgO/CaO catalyst at 1023, K, W/F = 0.02 g-cat · h · mol^{-1}.

tively, without catalyst under the same reaction conditions. Hence the results shown in Fig. 1 reflects the activity of the oxides. Both the activity and the selectivity for C_2 were highest at 85% MgO/CaO, giving a total methane conversion of 13.6% and C_2 selectivity of 67.1%. Methane conversion to CO_x is only slightly affected by the catalyst composition, contrary to C_2 formation. By incorporating CaO into MgO an active site for C_2 formation should be generated independently of an active site for CO_x.

b. Effects of reaction temperature. In Table 1 are shown the temperature effects on the catalytic performances of 85% MgO/CaO catalyst, which showed the highest activity and selectivity among the mixed oxides at 1023 K. The selectivity for C_2 increased with the rise in reaction temperature up to 12.5% at 1103 K because the formation rate of C_2 increased while that of CO_x was constant.

TABLE 1

Effect of Reaction Temperature on 85% MgO/CaO

Temperature (K)	1003	1023	1043	1073	1103
	Conversion (%)				
CH_4	14.4	16.5	15.2	13.9	15.0
O_2	95.3	98.5	97.9	99.9	99.8
	CH_4 conversion rate (mmol · g^{-1} · h^{-1})				
C_2H_6	8.8	10.6	11.7	12.8	12.5
C_2H_4	3.3	4.7	5.1	6.3	6.5
CO	1.6	1.2	1.1	0.9	0.6
CO_2	6.3	6.3	6.7	6.8	6.6
C2 selectivity (%):	60.4	67.1	68.4	71.5	72.5

Note. W/F = 0.85 g-cat · h · mol^{-1}, P_{CH_4} = 13.1 kPa, P_{O_2} = 1.4 kPa, P_{N_2} = 86.5 kPa.

c. Reaction orders with respect to partial pressure of CH_4 and O_2. Reaction orders were examined under differential conditions where conversion of both CH_4 and O_2 were always less than 10%. Nitrogen was used as balance gas to control the partial pressure. Figure 2 demonstrates the dependence of the formation rate of C_2 and CO_x with 85% MgO/CaO catalyst. Ethane was predominant (>90%) in the C_2 hydrocarbons in every case. Since experimental results showed good linearity between the pressure and the rate, a power rate law expression can be applied. Solid lines in Fig. 2 correspond to rates calculated by Eqs. (1) and (2), where r_{C_2} and r_{CO_x} are formation rates (mmol · h^{-1} · g^{-1}) of C_2 and CO_x, respectively, and P_{CH_4} and P_{O_2} are partial pressure (kPa) of methane and oxygen, respectively:

$$r_{C_2} = 32 \cdot P_{CH_4}^{0.3} \cdot P_{O_2}^{0.0} \quad (1)$$

$$r_{CO_x} = 60 \cdot P_{CH_4}^{0.0} \cdot P_{O_2}^{0.9}. \quad (2)$$

It is clear that a high partial pressure of methane and a low partial pressure of oxygen are favorable for high C_2 selectivity.

Structural and Morphological Features

Specific surface areas of CaO/MgO mixed oxides increase from pure CaO (31 $m^2 \cdot g^{-1}$) with increasing MgO content to reach a maximum value (62 $m^2 \cdot g^{-1}$) at 50% MgO/CaO and then decrease almost proportionally with MgO content to reach 18 $m^2 \cdot g^{-1}$ at pure MgO (Fig. 1). The variation of specific surface area as a function of catalyst composition is quite similar to that of CO_2 uptake at room temperature. This means that on each oxide surface, CO_2 is adsorbed. The values do not correlate with catalytic activity.

XRD measurements of the mixed oxides show exclusively the diffraction pattern of MgO (periclase) and CaO. No peaks attributable to the hydroxides or carbonates were found. Calculation of lattice constants according to the method described in Ref. (*14*) gives (4.80 ± 0.015) Å for CaO and (4.20 ± 0.100) Å for MgO independent of catalyst composition and in agreement with literature data (*15, 16*). Doping of CaO leads to a remarkable broadening of the MgO peaks, whereas the CaO peaks become narrower. Peak positions are only slightly influenced in a unsystematic manner. Line breath of XRD reflections is affected both by particle size and microstrain inside the crystal lattice (*13, 14, 17*). According to Hall (*17*) the relationship between these parameters is expressed by

$$\beta \cos \Theta/\lambda = 1/\varepsilon + \eta \sin \Theta/\lambda, \qquad (3)$$

where β represents linewidth, Θ and λ denote reflection angle, and X-ray wavelength, ε is the average particle size, and η is the effective strain. Correlation of $\beta \cos \Theta$ versus $\sin \Theta$ according to Eq. (3) gives good straight lines with correlation higher than 0.98, except for 95% MgO/CaO sample (0.94 and 0.90). Values of ε and η can be calculated from the slope and the intercept, respectively. Their dependences on catalyst composition are shown in Fig. 3. The particle sizes of the MgO crystallites increase with increasing CaO content to reach maximum at 5% CaO, then decrease at higher CaO amounts. The size of CaO particles is highest for the 50% MgO/CaO sample. The stress effect in the MgO crystallites is strongest in the 85% MgO/CaO sample, whereas that of the CaO crystallites is highest for the 50% MgO/CaO catalyst. The results show that the composition of the catalyst affects their crystallographic properties, although a uniform and common MgO/CaO phase is not formed.

Adsorption and Desorption of CO_2

The basicities of the mixed oxides were investigated using CO_2 adsorption. The volumetrically measured CO_2 uptake on mixed oxides was larger than that of pure CaO or pure MgO. The amount increases linearly with increasing CaO content in MgO and vice versa in CaO catalyst. A significant relationship between CO_2 uptake and activity was not observed.

TPD of CO_2 was conducted to clarify the adsorption strength of CO_2 since a desorption peak at high temperature corresponds to high basicity of the surface. The desorption profiles in Fig. 4 are classified into two categories of CaO-rich catalyst and MgO-rich catalyst. CaO-rich samples (0% MgO/CaO and 50% MgO/CaO) showed almost the same desorption profile up to 673 K and the same activity for C_2 formation (Fig. 1). It could be concluded that the incorporation of MgO into CaO contributed only slightly to the increase in its activity and basicity.

Contrary to CaO-rich catalysts, MgO-rich catalysts were effectively modified by the incorporation of CaO. The characteristic peak between 873 and 973 K was most remarkable on 85% MgO/CaO among the MgO-rich oxide catalysts. These observation suggest that the high activity of 85% MgO/CaO arises from a high basicity originating from surface structure. To obtain information on the character of the adsorption state, FTIR spectroscopic measurements were performed.

IR Spectroscopic Measurement of Adsorbed CO_2

a. Adsorption states at room temperature. Figure 5 shows spectra of calcined

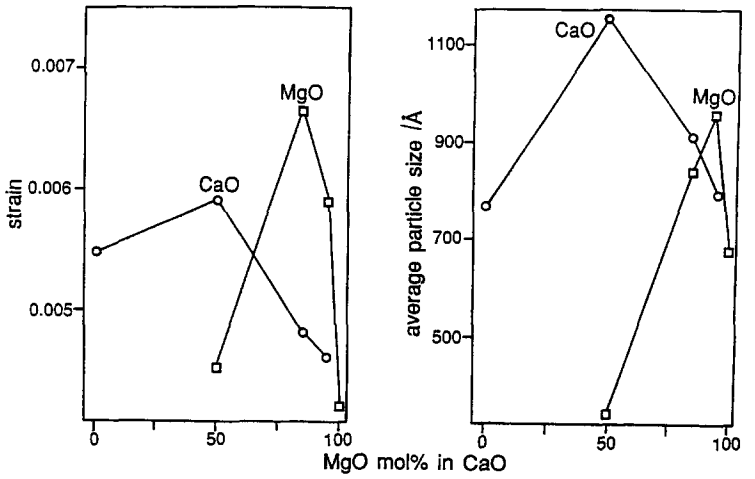

FIG. 3. Dependence of average particle sizes and microstrains on catalyst composition.

MgO, 85% MgO/CaO, 50% MgO/CaO, and CaO before and after CO_2 exposure and after heating at 373 K. The calcined samples produce absorption bands around 1000 cm^{-1} caused by crystal lattice vibrations (*18, 19*). No OH stretching bands of residual surface hydroxyl groups were detected on MgO-rich samples whereas on CaO and 50% MgO/CaO a weak band at 3640 cm^{-1} was found (not shown in the figure). However, it was proved by deuterium exchange reaction that even after outgassing MgO at 1273 K a measurable number of surface hydroxyls remains on the surface (*20*). It can also be assumed that under reaction conditions the water molecules formed create a small population of surface hydroxyls.

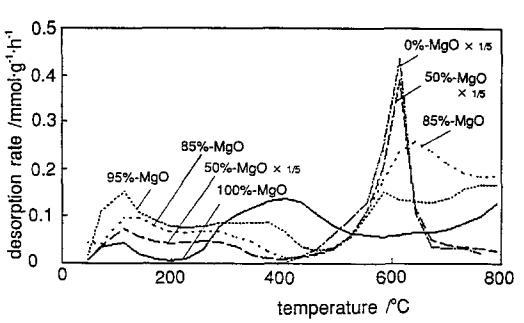

FIG. 4. Desorption profile of CO_2 at 10 K · min^{-1}.

Adsorbed CO_2 produces large bands in the range 1400 to 1550 cm^{-1} with a shoulder at still higher wavenumbers. A weaker band around 1070 cm^{-1} and a very weak one around 1220 cm^{-1} are observed. On 50% MgO/CaO and pure CaO additional bands around 1780, 2500, and 2900 cm^{-1} appear. The bands between 1400, and 1550, and 1070 cm^{-1} are attributed to surface unidentate carbonates (Fig. 6) (*18, 19, 21, 22*) and belong to the antisymmetric and symmetric O_ICO_I stretching vibration and the stretching vibration of $O_{II}C$, respectively. Unidentate carbonate seems to be the dominant adsorption state of CO_2 at room temperature. The shoulder band at 1630–1660 cm^{-1} is most probably assigned to the antisymmetric stretching mode of O_ICO_{II} of a surface bicarbonate (*19, 21, 22*) (Fig. 6), which is formed by interaction of CO_2 with surface hydroxyl. The symmetric stretching vibration of O_ICO_{II} is reported to lie in the range 1410–1480 cm^{-1} (*19, 22, 23*). This means that in the present case this band is masked by the broad symmetric stretching mode of the unidentate complex. The weak band around 1220 cm^{-1} is probably caused by the COH bending vibration of bidentate (*19, 22, 23*). The band around 1780 cm^{-1} on CaO and 50% MgO/CaO is tentatively assigned

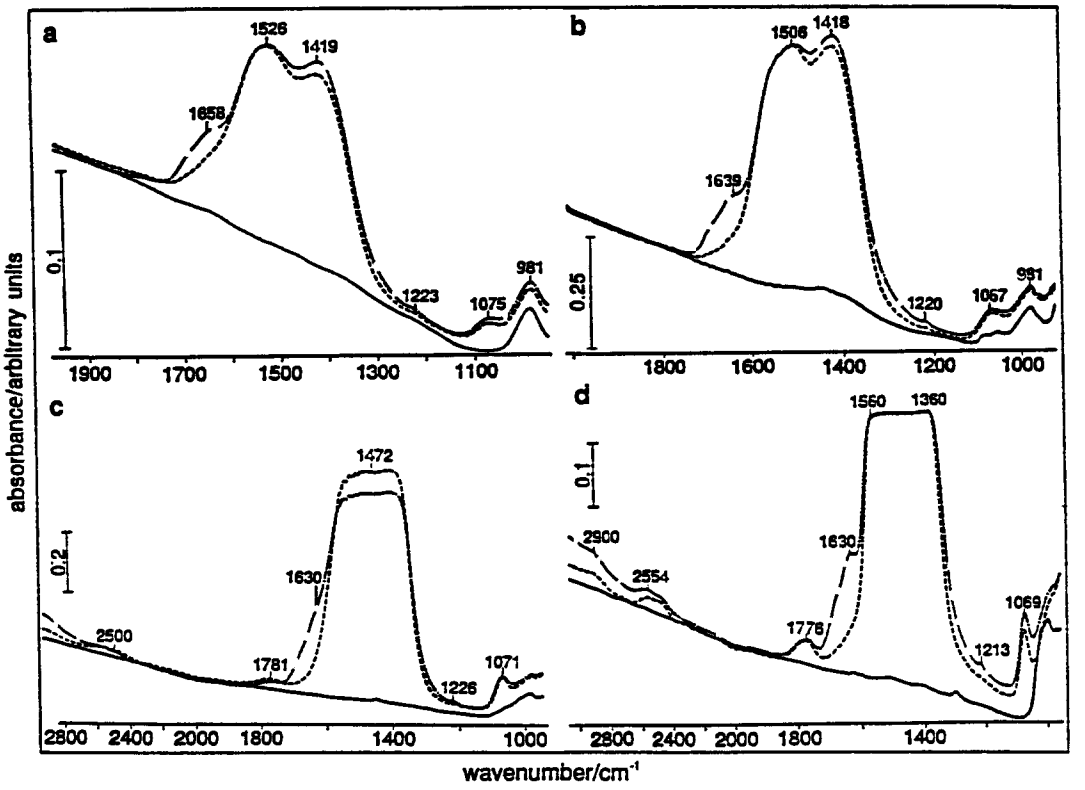

FIG. 5. FTIR spectra at room temperature for (a) MgO, (b) 85% MgO/CaO, (c) 50% MgO/CaO, (d) CaO, after calcination (—), subsequent exposure to CO_2 at room temperature (– –) and subsequent heating at 373 K (---).

to the CO_{II} stretching mode of a "bridging" carbonate (*21, 23–25*) (Fig. 6). For this structure an asymmetric stretching O_ICO_I band in the region 1150 to 1259 cm^{-1} is expected (*21, 23*). A weak shoulder band in this range is just discernible. The corresponding symmetric O_ICO_I stretching mode is reported to lie in the range 1020 to 970 cm^{-1} (*21*) and hence it is masked by metal oxide lattice vibrations. "Bridging" carbonate is known to be formed on different Al_2O_3-containing surfaces (*23–26*) but not yet for CaO (*13, 18*).

The bands at higher wavenumbers can hardly be explained by surface carbonates. More probably, they are caused by weaker adsorbed CO_2, where the molecules are assumed to interact via one oxygen atom with metal cations, preserving its linear shape. Such species are well known on Al_2O_3 (*23*) and mixed Al_2O_3/MgO surfaces (*22, 27*). They produce more than one band in the range 2250–2500 cm^{-1}. The bands observed in our case, however, have somewhat higher wavenumbers. The assignments are summarized in Table 2 and Fig. 6.

b. Desorption of CO_2. Heating the samples at 373 K leads to the disappearance of the shoulder band at 1630–1660 cm^{-1} and mostly to a slight decrease in the height of the main band between 1400 and 1550 cm^{-1} (Fig. 5). This indicates the desorption of the bicarbonate, which is known to have a lower thermal stability than unidentate carbonate (*22*). The result corresponds to the first peak (around 398 K) in the TPD spectrum (Fig. 4). These findings are independent of catalyst composition.

TABLE 2

Wavenumbers (in cm^{-1}) of Adsorbed CO_2 at Room Temperature and after Heating at Different Desorption Temperatures

	Room temp.	373 K	573 K	773 K	873 K
MgO	1075 A_1	1072 A_1			
	1419 A_2,B_2	1421 A_2	1393 A_2		
	1526 A_3	1522 A_3	1504 A_3		
	1658 sh B_3				
	1223 B_1				
95% MgO/CaO	1072 A_1	1068 A_1	1058 A_1	1069 A_1	1074 A_1
	1415 A_2,B_2	1414 A_2	1405 A_2	1427 A_2	around 1418 A_2
	1506 A_3	1513 A_3	1513 A_3	1481 A_3	1478 A_3
	1637 sh B_3				
	1220 B_1				
					1584
85% MgO/CaO	1067 A_1	1067 A_1	1060 A_1		
	1418 A_2,B_2	1420 A_2	1411 A_2	1418 A_2	
	1506 A_3	1509 A_3	1492 A_3	1478 A_3	around 1480 A_3
	1639 sh B_3				
	1217 B_1				
50% MgO/CaO	1071 A_1	1072 A_1	1053 A_1		
	around	around	around	around	1428 A_2
	1472 A_2,A_3,B_2	1477 A_2,A_3	1461 A_2,A_3	1455 A_2,A_3	1542 A_3
	1630 sh B_3				
	1220 B_1				
				1299 E_1	1304 E_1
				1624 E_2	1622 E_2
	1781 C_1	1782 C_1	1781 C_1	1797 C_1	
	2500 D	2500 D	2500 D	2518 D	
				2783 D	
CaO	1069 A_1	1073 A_1	1074 A_1	1063 A_1	
	around	around	around	around	1425 A_2
	1461 A_2,A_3,B_2	1470 A_2,A_3	1469 A_2,A_3	1458 A_2,A_3	1533 A_3
	1630 sh B_3				
	1213 B_1				
				1299 E_2	1299 E_2
				1629 E_1	1619 E_1
	1776 C_1	1780 C_1	1780 C_1	1797 C_1	
	2554 D	2550 D	2554 D	2514 D	
	2900 D	2880 D	2800 D	2877 D	
					1368

Note. sh, shoulder. A_1, A_2, A_3: CO_{II} stretching, O_ICO_I symmetric stretching, and O_ICO_I antisymmetric stretching mode of unidentate carbonate. B_1, B_2, B_3: COH bending, O_ICO_{II} symmetric stretching, and O_ICO_{II} antisymmetric stretching mode of bicarbonate. C_1: CO_{II} stretching mode of "bridging" carbonate. D: CO stretching modes of linearly adsorbed CO_2. E_1, E_2: CO_{II} stretching and O_ICO_I antisymmetric stretching mode of bidentate carbonate.

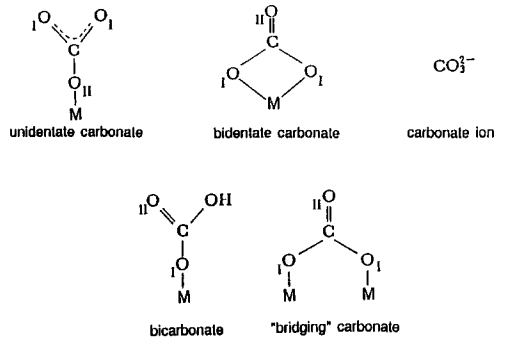

FIG. 6. Structures of surface carbonates, formed by adsorption of CO_2 on metal oxide MO (*18–21*).

In contrast, desorption temperatures of the unidentate carbonate increase with increasing CaO content. On pure MgO desorption starts around 473 K and most of the absorption bands disappear below 773 K (Fig. 7). This desorption process causes the second peak (673 K) in the TPD spectrum (Fig. 4). The unidentate carbonate on the MgO/CaO mixed oxides is stable over a wider temperature range than on pure MgO. For instance, the intensities of the corresponding bands on the 85% MgO/CaO sample diminish in the range 473 K $< T <$ 973 K (Fig. 7).

Absorption bands on 50% MgO/CaO and pure CaO do not change their shape below 673 K. At this temperature the three bands at higher wavenumbers start to develop sharp peaks. This effect continues at 773 K. Simultaneously, the band around 1470 cm^{-1} becomes narrower and starts to split, and the band around 1070 cm^{-1} decreases. This indicates the beginning of desorption of the unidentate carbonate whereby a small amount of it is converted into other surface species. It was already reported (*27, 28*) that increase in temperature and dehydration weakens the basicity of surface oxygen on Al_2O_3 and $MgAl_2O_4$. This leads to transformation of unidentate into bridging species, where an additional bond between one oxygen atom of CO_2 and metal cation stabilizes the surface structure. Also in the present case a decreased activity of surface oxygen may be the reason for the features mentioned above.

After heating to 873 K the broadband around 1470 cm^{-1} is drastically decreased and all bands at higher wavenumbers disappear. This is in accordance with the sharp peak in the TPD spectrum at 873 K (Fig. 4). The remaining bands decrease continuously with further increase in temperature. Even at 1073 K some of the bands between 1600 and 1350 cm^{-1} are still observed. The bands around 1535 and 1425 cm^{-1} are assigned to unidentate carbonate, whereas the band around 1300 cm^{-1} and the small shoulder band around 1620 cm^{-1} may be caused by traces of bidentate carbonate (asymmetric O_ICO_I stretching and CO_{II} stretching mode) for which the splitting of the asymmetric CO stretching mode of carbonate ion is reported to be ca. 300 cm^{-1} (*13, 18, 19, 21*). The coexistence of uni- and bidentate carbonate at higher temperatures and lower coverages was already found by Fukuda and Tanabe (*18*). All assignments are summarized in Table 2. Adsorption/desorption behavior of CO_2 on the 50% MgO/CaO sample is very similar to pure CaO, indicating that large parts of the surface are covered with CaO.

d. Correlation with surface basicity and catalytic activity. It was already reported that MgO formed by thermal decomposition of the hydroxide consists of agglomerates of crystallites with high densities of higher index planes and consequently larger numbers of low coordinate oxide ions (*29, 30*). These high-index planes are more selective for C_2 hydrocarbon formation compared to low-index crystallographic planes (*29*).

The IR-spectroscopic results show that on pure MgO and on MgO doped with small amounts of CaO the same CO_2 adsorption states are formed. This means that the surfaces of these samples consist mainly of MgO. However, higher amounts of adsorbed CO_2 and enhanced thermal stability of the adsorbate reflect that the surfaces are modified by CaO; this CaO is probably highly dispersed so that a large boundary

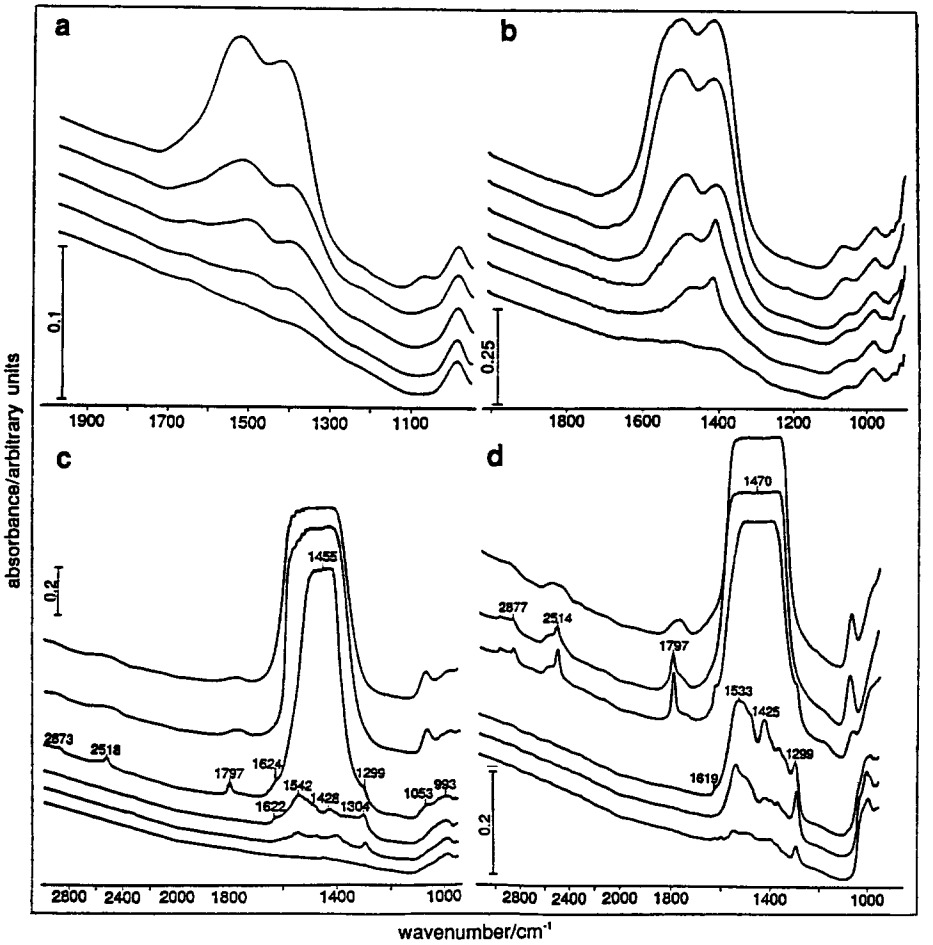

FIG. 7. FTIR spectra at room temperature after CO_2 adsorption (a) on MgO after subsequent heating at 373, 523, 573, 676, 773 K; (b) on 85% MgO/CaO after subsequent heating at 373, 473, 573, 673, 773, 873 K; (c) on 50% MgO/CaO after subsequent heating at 373, 673, 773, 873, 973, 1073 K; (d) on CaO after subsequent heating at 443, 673, 773, 873, 973, 1073 K.

region between MgO and CaO exists. This modification causes changes in morphology and surface basicity, as discussed later. On the other hand, on CaO-rich sampels (including the 50% MgO/CaO sample) CO_2 forms the same adsorption states as on pure CaO, indicating that the surfaces are largely covered by CaO and not effectively modified by incorporated MgO. These findings are in agreement with previous morphological studies of the MgO system. Calcium segregation to MgO surfaces was theoretically predicted (*31*) and spectroscopically proved (*32, 33*). In contrast, a depletion of Mg^{2+} was predicted at low-index planes of CaO (*31*).

Enrichment of Ca^{2+} on the surface of MgO leads to surface reconstruction processes that create a "rumpled" arrangement with oxygen anions displaced outward (*11, 31, 34*) and higher densities of surface ions in lower coordination (*33, 34*). These anions are catalytically more reactive. For higher CaO levels the CaO content is large enough to form more than one monolayer of CaO on MgO. In this case the misfit between the

surface monolayer and the underlying layer is less and consequently the reconstructed surface is less rumpled in structure. This may be the reason for the decline in catalytic activity of the oxides in which the Ca content reaches levels higher than 25%.

Surface rumpling is probably not the only factor that governs catalytic activity; otherwise MgO covered with a monolayer of CaO should be the catalytically most active sample. However, on such a sample adsorbed CO_2 should form adsorption states like those on pure CaO. In the present case, on the catalytically most active samples adsorption states are similar to those formed on pure MgO. We conclude, therefore, that besides surface rumpling the boundary region between CaO and MgO creates sites with enhanced reactivity. This region is largest for highly dispersed CaO.

The connection between strain and catalytic activity indicates that segregation and surface reconstruction are incomplete on the high-index planes that form the surface of the catalyst. This is in agreement with Ref. (*34*), in which it was proved that on polycrystalline MgO surfaces doped with Ca^{2+} rumpled regions coexist with nonreconstructed regions. Possibly, the increased strain indicates a larger number of defects on the surface, which may be involved in catalytic reactions. Increased lattice strain resulting in high C_2 selectivities was already reported for MgO catalysts doped with Na^+ (*3*). In this case, the lattice distortion was considered to create surface active centers for methyl radical formation.

It was reported (*18, 22, 35*) that the wavenumber difference $\Delta\nu = \nu_{as} - \nu_{sy}$ of the asymmetric and symmetric stretching band of surface carbonates decreases with increasing (more negative) partial charge of the lattice oxygen, i.e., increasing electron-pair donor properties. This means that the degree of $(\Delta\nu)^{-1}$ seems to be a direct measure of the strength of Lewis-basic sites. In Fig. 8 $(\Delta\nu)^{-1}$ is shown as a function of MgO content. It is clear from the data that addition of small doses of CaO increase the

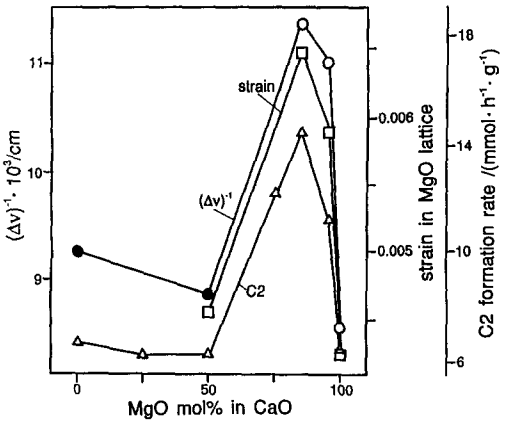

FIG. 8. Correlation of the reciprocal value of the wavenumber difference ($\Delta\nu$) of the asymmetric and symmetric CO stretching band, of the strain in the MgO lattice, and of the C_2 formation rate versus MgO content. $(\Delta\nu)^{-1}$ values were obtained at room temperature (○) and after heating at 873 K (●).

Lewis basicity of the MgO surface, remarkably. For the 50% MgO/CaO sample and for pure CaO, $\Delta\nu$ could be obtained only after heating the sample at temperatures equal to or higher than 873 K. At lower temperatures the band concerned does not show any fine structure. However, the values indicate a decrease in surface basicity in comparison to the samples with smaller CaO amount.

Figure 9 shows that the catalyst properties of strain, number of strong basic sites, and Lewis basicity increase monotonically with the activity increment (C_2 formation rate minus C_2 formation rate on pure MgO). These results show that small amounts of CaO increase basicity and modify the morphology of MgO surfaces. Both properties seem to enhance the catalytic activity toward methane coupling.

CONCLUSION

By studying the catalytic performances, the morphologies, and the characteristics of adsorbed CO_2 on mixed MgO/CaO oxide catalysts the following conclusions were obtained:

(1) The mixed oxides that contain 10 to

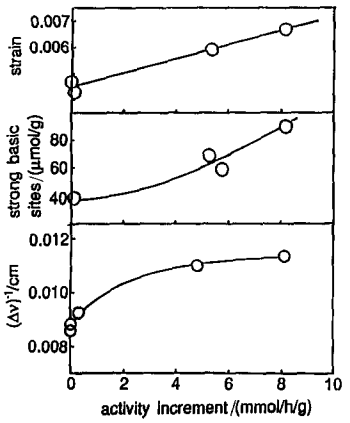

FIG. 9. Correlation of microstrain, number of strong basic sites, and reciprocal value of the wavenumber difference of symmetric and asymmetric stretching band versus activity increment.

15% of CaO exhibited extraordinarily high activities and selectivities for C_2 formation.

(2) The high activity arose from MgO modified by CaO.

(3) Surfaces of the MgO-rich oxides were covered mostly by MgO and its basicity was enhanced by incorporated CaO.

(4) The enhanced basicity of MgO is connected with morphological changes in the surface layer.

(5) The basicity of the mixed oxides was well characterized by the IR wavenumber difference of asymmetric and symmetric stretching of surface carbonate.

REFERENCES

1. Carreiro, J. A. S. P., and Baerns, M., *J. Catal.* **117,** 258 (1989).
2. DeBoy, J. M., and Hickes, R. F., *Ind. Eng. Chem. Res.* **27,** 1577 (1988).
3. Iwamatsu, E., Moriyama, T., Takasaki, N., and Aika, K., *J. Catal.* **113,** 25 (1988).
4. Ito, T., Wang, J.-X., Liu, C.-H., and Lunsford, J. H., *J. Am. Chem. Soc.* **107,** 5062 (1985).
5. Driscoll, D. J., Martir, W., Wang, J.-X., and Lunsford, J. H., *J. Am. Chem. Soc.* **107,** 58 (1985).
6. Peng, X. D., Richards, D. A., and Stair, P. C., *J. Catal.* **121,** 99 (1990).
7. Matsuda, T., Minamino, Z., Shibata, Y., Nagano, S., Miura, H., and Sugiyama, K., *J. Chem. Soc., Faraday Trans. 1* **82,** 1357 (1986).
8. Yamagata, N., Tanaka, K., Sasaki, K., and Okazaki, S., *Chem. Lett.*, 81 (1987).
9. Choudhatry, V. R., Chaudhari, S. T., Rajput, A. M., and Rane, V. H., *J. Chem. Soc., Chem. Commun,* 555 (1989).
10. Fujimoto, K., Hashimoto, S., Asami, K., Omata, K., and Tominaga, H., *Appl. Catal.* **50,** 223 (1989).
11. Cunningham, J., Healy, C., McNamara, D., and O'Brien, S., *Catal. Today* **2,** 557 (1988).
12. Omata, K., Aoki, A., and Fujimoto, K., *Catal. Lett.* **4,** 241 (1990).
13. Matsukata, M., Okanari, E., Kobayashi, K., Kikuchi, E., and Morita, Y., *Sekiyu Gakkaishi* **32,** 97 (1989).
14. Warren, B. E., "X-Ray Diffraction," Chap. 13. Addison-Wesley, Reading, MA, 1969.
15. Dowden, D. A., *in* "Catalysis Reviews" (H. Heinemann, Ed.), Vol. 5, p. 5, pp. 1386–1388. Dekker, New York, 1972.
16. Cotton, F. A., and Wilkinson, G., "Advanced Inorganic Chemistry," 5th ed. pp. 1386–1388. Wiley, New York, 1988.
17. Hall, W. H., *Proc. Phys. Soc A* **62,** 741 (1949).
18. Fukuda, Y., and Tanabe, K., *Bull. Chem. Soc. Jpn.* **46,** 1616 (1973).
19. Evans, J. V., and Whateley, T. L., *Trans. Faraday Soc.* **63,** 2769 (1967).
20. Zhang, G., and Hattori, H., *in* "Acid–Base Catalysis" (K. Tanabe, H. Hattori, T. Yamaguchi, and T. Tanaka, Eds.), pp. 475–482. Kodansha, Tokyo, 1989.
21. Little, L. H., "Infrared Spectra of Adsorbed Species," pp. 76–77. Academic Press, London, 1966.
22. Lercher, J. A., Colombier, C., and Noller, H., *J. Chem. Soc., Faraday Trans. 1* **80,** 949 (1984).
23. Morterra, C., Zecchina, A., Coluccia, S., and Chiorino, A., *J.Chem. Soc., Faraday Trans. 1* **73,** 1544 (1977).
24. Parkyns, N. D., *J. Chem. Soc. A,* 410 (1969).
25. Parkyns, N. D., *J. Phys. Chem.* **75,** 526 (1971).
26. Little, L. H., and Amberg, C. H., *Can. J. Chem.* **40,** 1997 (1962).
27. Morterra, C., Chiorino, A., Boccuzzi, F., and Coluccia, S., *J. Catal.* **51,** 299 (1978).
28. Morterra, C., Coluccia, S., Ghiotti, G., and Zecchina, A., *Z. Phys. Chem. (N. F.)* **104,** 275 (1977).
29. Hargreaves, J. S. J., Hutchings, G. J., and Joyner, R. W., *Catal. Today* **6,** 481 (1990).
30. Coluccia, S., Tench, A. J., and Segall, R. L., *J. Chem. Soc., Faraday Trans 1* **75,** 1769 (1979).
31. Tasker, P. W., Colbourn, E. A., and Mackrodt, W. C., *J. Am. Chem. Soc.* **68,** 74 (1985).
32. McCune, R. C., and Wynblatt, P., *J. Am. Ceram. Soc.* **66,** 111 (1983).

33. Zecchina, A., Lofthouse, M. G., and Stone, F. S., *J. Chem., Soc., Faraday Trans. 1* **71,** 1476 (1975).
34. Cunningham, J., O'Brien, S,. McNamara, D., Bourke, M., and Egdell, R., *in* "Proceedings, 9th International Congress on Catalysis, Calgary, 1988" (M. J. Phillips and M. Ternan, Eds.), Vol. 4, p. 1719. Chem. Institute of Canada, Ottawa, 1988.
35. Sanderson, R. T., "Chemical Bond and Bond Energy." Academic Press, New York, 1965.